Observation of Degradation of Pt and Carbon Support in Polymer Electrolyte Fuel Cell Using Combined Nano-X-ray Absorption Fine Structure and Transmission Electron Microscopy Techniques

doi: 10.1021/acsami.8b04407

Observation of Degradation of Pt and Carbon Support in Polymer Electrolyte Fuel Cell Using Combined Nano-XAFS and TEM Techniques

Shinobu Takao,[a] Oki Sekizawa,[a] Gabor Samjeské,[a] Takuma Kaneko,[a] Kotaro Higashi,[a] Yusuke Yoshida,[a] Xiao Zhao,[a] Tomohiro Sakata,[a] Takashi Yamamoto,[b] Takao Gunji,[a] Tomoya Uruga,[a, c] and Yasuhiro Iwasawa [a, d]∗

[a] Innovation Research Center for Fuel Cells, The University of Electro-Communications, Chofu, Tokyo 182-8585, Japan

[b] Department of Mathematical and Material Sciences, Faculty of Integrated Arts and Sciences, The University of Tokushima, Minamijosanjima, Tokushima 770-8502, Japan

[c] SPring-8, Japan Synchrotron Radiation Research Institute, Sayo, Hyogo 679-5198, Japan

[d] Department of Engineering Science, Graduate School of Informatics and Engineering, The University of Electro-Communications, Chofu, Tokyo 182-8585, Japan

Abstract

It is hard to directly visualize spectroscopic and atomic–nanoscopic information on the degraded Pt/C cathode layer inside polymer electrolyte fuel cell (PEFC). However, it is mandatory to understand the preferential area, sequence and relationship of the degradations of Pt nanoparticles and carbon support in the Pt/C cathode layer by directly observing the Pt/C cathode catalyst for development of next-generation PEFC cathode catalysts. Here, the spectroscopic, chemical and morphological visualization of the degradation of Pt/C cathode electrocatalysts in PEFC was performed successfully by a same-view combination technique of nano-XAFS and TEM/STEM-EDS under a humid N_2 atmosphere. The same-view nano-XAFS and TEM/STEM-EDS imaging of the Pt/C cathode of PEFC after triangular-wave 1.0–1.5 V_{RHE} (startup/shutdown) accelerated durability test (tri-ADT) cycles elucidated the site-selective area, sequence and relationship of the degradations of Pt nanoparticles and carbon support in the Pt/C cathode layer. The 20 tri-ADT cycles caused a carbon corrosion to reduce the carbon size preferentially in the boundary regions of the cathode layer with both electrolyte and holes/cracks, accompanied with detachment of Pt nanoparticles from the degraded carbon. After the decrease in the carbon size to less than 8 nm by the 50 tri-ADT cycles, Pt nanoparticles around the extremely corroded carbon areas were found to transform and dissolve into oxidized Pt^{2+}-O_4 species.

Keywords: Same-view imaging, Nano-XAFS/STEM-EDS, PEFC Pt/C cathode, Pt and carbon degradations, Degradation sequence

Introduction

Hydrogen fuel cell is one of clean and efficient power generation systems for future hydrogen vehicles, sustainable low-carbon society, diverse energy security, *etc*. For the widespread commercialization of polymer electrolyte fuel cell (PEFC) vehicles, however, both performance and long-term durability of the current Pt/C cathode electrocatalysts are insufficient for the sluggish oxygen reduction reaction (ORR), and hence, remarkable improvements of both ORR activity and long-term durability are indispensable.[1–5] For example, the DOE 2020 mass activity (MA) and durability targets are presented to be 0.44 A mg^{-1}_{Pt}@0.9 V_{RHE} after electrochemical conditioning (activation) and 0.26 A mg^{-1}_{Pt}@0.9 V_{RHE} after rectangular-wave 0.6–1.0 V_{RHE} 30,000 cycles, respectively.[6] Particularly, the degradation of cathode electrocatalysts due to carbon corrosion and Pt dissolution and detachment during startup/shutdown cycles should be significantly suppressed.[7-10] Any Pt-based electrocatalysts with high ORR performance and durability, particularly long-term durability against startup/shutdown load cycles (simulated by triangular-wave 1.0–1.5 V_{RHE} cycles), have not been reported thus far. For development of next-generation PEFC cathode electrocatalysts, it is mandatory to understand the preferential area, sequence and relationship of the degradations of Pt nanoparticles and carbon support in the Pt/C cathode layer of membrane electrode assembly (MEA) in PEFC by directly observing the MEA Pt/C cathode electrocatalyst.

An assumed schematic diagram of the degradation of MEA Pt/C cathode under 1.0–1.5 V_{RHE} voltage operation (startup/shutdown cycles) is shown in Scheme 1. It has been suggested from electrochemical points of view that at first carbon corrosion and Pt-catalyzed carbon oxidation occur, and subsequently Pt nanoparticles degrade due to particle growth, aggregation, detachment and dissolution.[11-14] However, there is no direct evidence

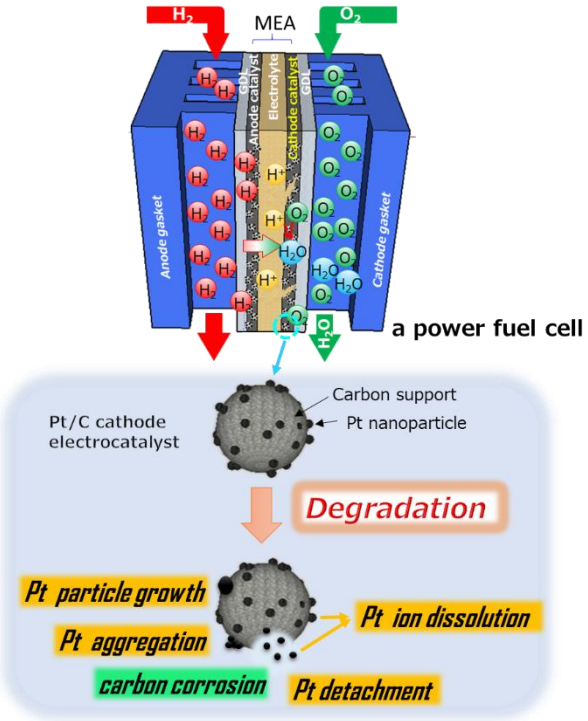

Scheme 1. An assumed schematic diagram of the degradation of the Pt/C cathode electrocatalyst in membrane electrode assembly (MEA) of polymer electrolyte fuel cell (PEFC) under 1.0–1.5 V_{RHE} voltage operations (startup/shutdown cycles).

of the easy sites, sequence and mechanism of the cathode degradation because there are few suitable *in situ* and *ex situ* analysis methods to elucidate the corrosion, structures and chemical states of Pt/C cathode electrocatalysts with nanometer dimensions inside MEA of PEFC. It is hard to directly visualize spectroscopic and atomic–nanoscopic information on the degraded Pt/C cathode layer inside MEA.

In situ and time-resolved X-ray absorption fine structure (XAFS) techniques are recognized to enable element-selective investigation on the local structures and oxidation states of Pt/C, Pt_3Co/C and Pt_3Ni/C cathode electrocatalysts in PEFC.[15,16] The time-resolved quick XAFS can also decide ORR elementary steps and their rate constants under voltage transient response processes.[15–26] The *in situ* and time resolved QXAFS can provide

structural and electronic information on cathode electrocatalysts in MEA, which cannot be obtained by other analysis techniques, but the information is averaged in a larger than ten-micrometers area of the cathode irradiated with non-focusing X-rays. The key elementary processes and degradation of the Pt/C cathode, which regulate the ORR activity and durability of PEFC, have been visualized to occur heterogeneously in the space of the cathode layer by a 3D Laminography-XAFS method with 1 μm spatial resolution.[27] The degradation of carbon supports under startup/shutdown processes for PEFCs has also been reported.[28]

Recently, we have developed a same-view membrane cell, which allows the simultaneous view of both Pt valence/bonding states by nano-XAFS and elemental distribution/carbon corrosion by TEM/STEM-EDS under a humid N_2 atmosphere by combining the nano-focusing XAFS and TEM/STEM-EDS.[29-31] The combination technique in the same-view cell provided spatial imaging information on the distribution of Pt nanoparticles and their oxidation states and coordination structures with chemical bonding in the Pt/C cathode electrocatalyst.[29-31] In the previous work, we investigated the heterogeneous degradation of Pt nanoparticles in the cathode layer after the rectangular-wave (0.6–1.0 V_{RHE}) accelerated durability test (rect-ADT) treatment.[29-31] While the results clearly showed the easy boundary areas to degrade, it was hard to separate and elucidate the nanoscopic degradation sequence at different sorts of boundary regions because the carbon corrosion and Pt deterioration occurred simultaneously. There is little information on the spatially heterogeneous issue, sequence and mechanism for the nanoscopic Pt detachment and dissolution closely related to the carbon corrosion in the Pt/C cathode catalyst layers.

Herein, we report direct visualization of the preferential areas, sequence and

relationship of the nanoscopic degradations of Pt nanoparticles and carbon support in MEA Pt/C cathode electrocatalysts, which was performed successfully by the same-view nano-XAFS and TEM/STEM-EDS imaging technique. The scanning nano-XANES and nano-EXAFS methods were used to spatially image Pt valences and bonding states, respectively. Nano X-ray beams with 210 x 226 nm^2 and 142 x 159 nm^2 sizes at SPring-8 BL36XU beamline that we designed and constructed for fuel cell research were used in this study.[15,23,32]

Results and discussion

The MEA Pt/C samples with different degrees of degradation were produced by the accelerated degradation test (ADT) procedure with triangular-wave 10, 20 and 50 cycles between 1.0 and 1.5 V_{RHE}. The activated (aging) Pt/C and the 10 tri-ADT degraded Pt/C in same-view membrane cells were imaged by STEM in Figure 1, which shows spatially heterogeneous degradation. Figure 1 displays a schematic same-view membrane cell (A) that we developed (Figure S1 in more detail) and STEM images (B–F) of wet sliced MEA Pt/C samples after aging (B) and 10 tri-ADT cycles at different places of the Pt/C cathode layer (C–F). The same-view stacking membrane cell has allowed us to achieve non-destructive TEM/STEM-EDS measurements under a humid N_2 atmosphere to avoid MEA transformations and destructions, which are easily caused by shrinking of ionomers and electrolytes by drying and water loss under high vacuum conditions taken for usual TEM/STEM-EDS observations.[29,30] After the electrochemical procedures, the PEFC was left under N_2 flows at both anode and cathode until it reached an open circuit voltage to prevent the sample from being exposed to high potentials. The MEA was sliced to a small piece with 200 nm thickness (4–6 layers of carbon particles) by an ultra-microtome under

a humid N_2 atmosphere, and the sliced MEA piece was putted on a 100 nm thick SiN membrane under a humid N_2 atmosphere. The resultant nano-XAFS spectra and TEM/STEM-EDS images for the sliced MEA in the SiN membrane stacking cell are regarded to be equivalent to those measured in situ after the aging and the ADT cycles

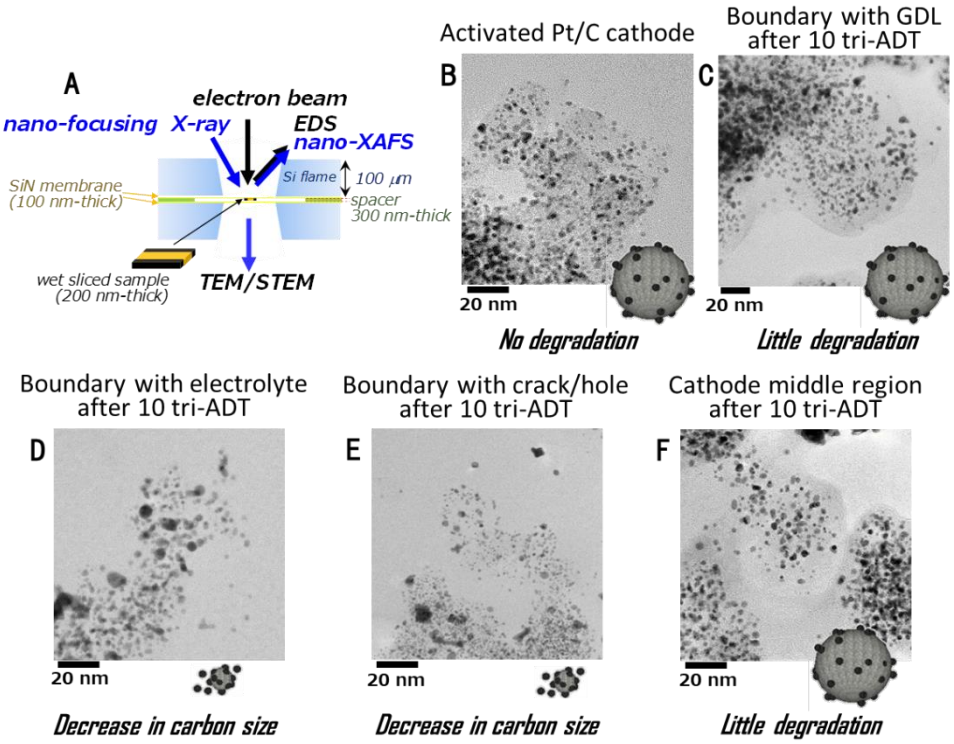

Figure 1. Schematic same-view membrane cell and STEM images of the cathode layer of wet sliced MEA Pt/C samples after aging (**B**) and 10 tri-ADT degradation (C-F). (**A**) Same-view membrane cell with a sliced MEA piece mounted on a 100 nm-thick SiN membrane for nano-XAFS/STEM-EDS. (**B**-**F**) **B**: STEM image of an activated MEA Pt/C cathode layer in the boundary region with the electrolyte after aging (0 tri-ADT cycle), **C**: STEM image of an MEA Pt/C cathode layer in the boundary region with the GDL after 10 tri-ADT cycles, **D**: STEM image of an MEA Pt/C cathode layer in the boundary region with the electrolyte after 10 tri-ADT cycles, **E**: STEM image of an MEA Pt/C cathode layer in the boundary region with the crack/hole after 10 tri-ADT cycles, and **F**: STEM image of the middle region of an MEA Pt/C cathode layer after 10 tri-ADT cycles. The initial size of carbon support is about 40 nm.

because all the procedures were conducted under the humid N_2 atmosphere without exposing air and the degradation of MEAs is irreversible in the present time scale.[30,31]

STEM image observations were performed in the boundary regions of the Pt/C cathode

layer with the gas diffusion layer (GDL) (Figure 1 C), the polymer electrolyte (Figure 1 D) and cracks/holes (Figure 1 E), and in the middle of the Pt/C cathode layer (Figure 1 F). The initial size of carbon nanoparticles after activation (aging) before the tri-ADT cycle is about 40 nm. After 10 tri-ADT cycles, the size of carbon supports reduced to 15–20 nm, and it was also observed that Pt nanoparticles detached from carbon surfaces in the 100 nm-wide boundary regions of the cathode layer with the polymer electrolyte (Figure 1 D) and cracks/holes (Figure 1 E). In the boundary region with the GDL and in the middle region of the cathode layer, however, there was only few change in the size of carbon nanoparticles and there was few detachment of the Pt nanoparticles (Figure 1 C and F). Thus, these results indicate that the carbon deterioration and Pt detachment occur site-selectively in the boundary regions with the electrolyte and cracks/holes.

Figure 2 shows the statistics data for the site-selective degradations of carbon support (Figure 2 A) and Pt catalyst nanoparticles (Figure 2 B). As the number of tri-ADT cycles

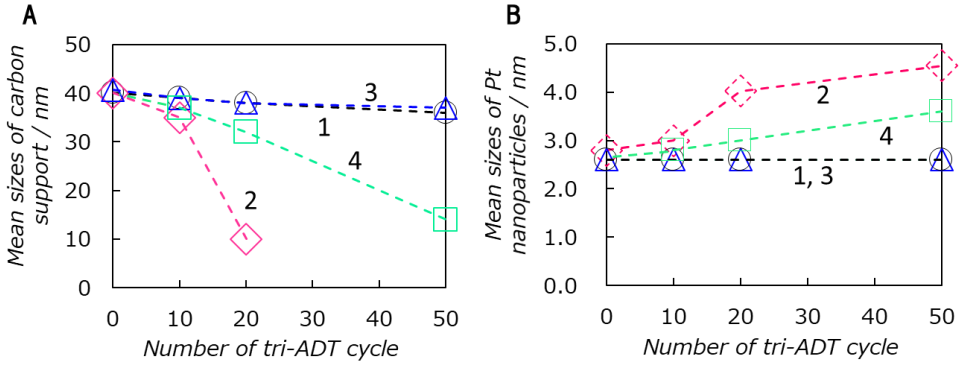

Figure 2. Degradations of carbon support and Pt nanoparticles in the Pt/C cathode catalyst layer; **A**: Variation of the mean size of carbon support with tri-ADT cycles, and **B**: Variation of the mean size of Pt nanoparticle with tri-ADT cycles. 1 (○): Middle of the cathode layer, 2(◇): 100 nm-wdie boundary region with the electrolyte, 3(△): 100 nm-wide boundary region with the GDL side, 4(□): 100 nm-wide boundary region with the cracks/holes. After 50 tri-ADT cycles, the carbon support morphology became unusual and it was difficult to measure the size, while a few nanometers of graphite structure were observed.

increased, the mean particle size of the carbon support in the MEA Pt/C cathode layer decreased from 40 nm to 10–14 nm preferentially in the 100 nm-wide boundary regions faced to the electrolyte and cracks/holes. Also in the boundary region of the cathode with the electrolyte and cracks/holes, the mean size of Pt nanoparticles increased from 2.8 nm to 4.5 nm and from 2.7 nm to 3.6 nm, respectively. Such site-selective degradation of both

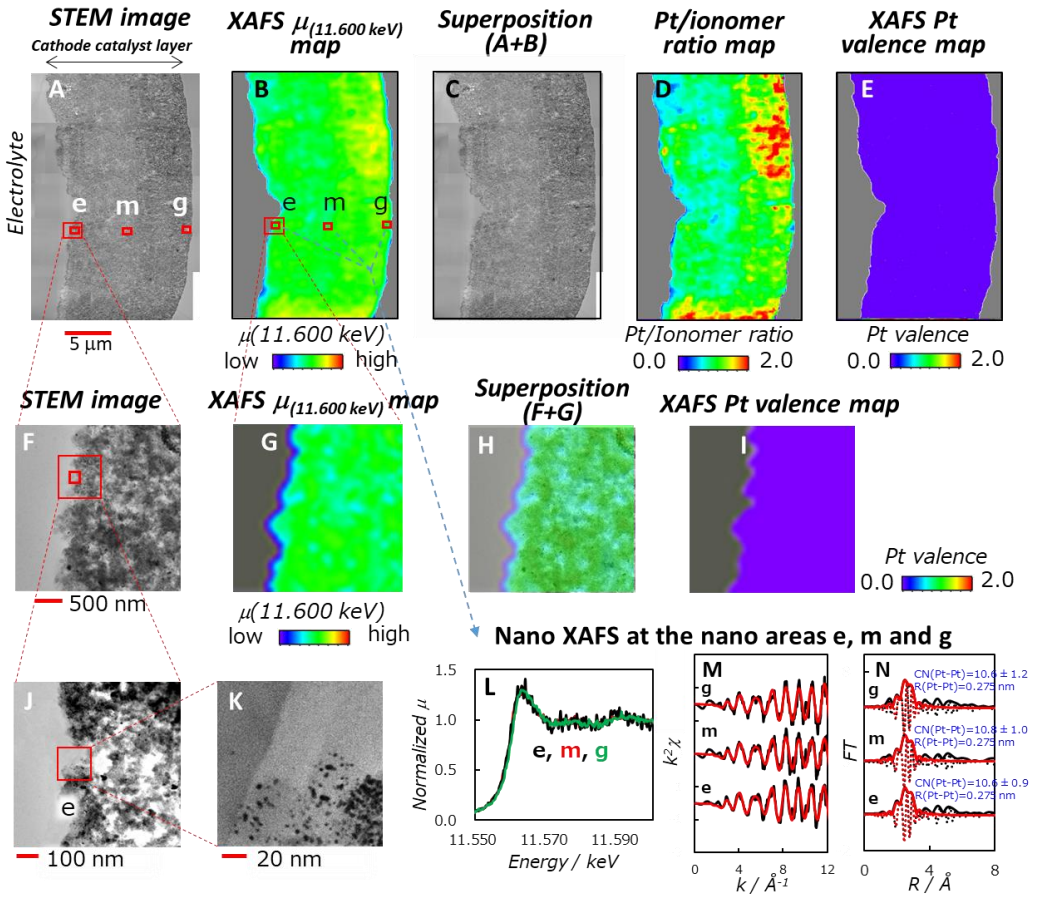

Figure 3. The same-view nano-XAFS/STEM-EDS imaging of the activated (aging) MEA cathode electrocatalyst for the 32 x 18 μm^2 (**A** - **E**) and 3 x 3 μm^2 regions (**F** - **I**). **A** and **F**: STEM images; **B** and **G**: XAFS absorbance $\mu_{(11.600\ keV)}$; **C** and **H**: the superpositions of **A** and **B** and **F** and **G**, respectively; **D**: map of Pt/Ionomer ratios; **E** and **I**: XAFS Pt valence maps; **J** and **K**: STEM images for the indicated red square areas; **I**: XAFS Pt valence map for **G**. **L**: nano XANES for the nano-square areas **e** (black), **m** (red), and **g**(green) shown in **A**. **M** and **N**: nano-EXAFS oscillations (**M**) and Fourier transforms (**N**) and their fittings (red); CN(Pt-Pt) and R(Pt-Pt) are shown in **N** (see Figure S2 and Table S1). The beam sizes are 210 x 226 nm and 142 x 159 nm for **B** - **E** and **G** – **I**, respectively

Pt nanoparticles and carbon support may be caused by spatially non-uniform potential loading and hydrogen fluoride formed by Nafion electrolyte deterioration.[33,34]

The STEM images and nano-XAFS maps around the cathode electrocatalyst layer after 0, 10, 20, 50 tri-ADT cycles are shown in Figures 3, 4, 5, and 7, respectively, where the STEM-EDS and nano-XAFS imagings in the same areas of the MEA Pt/C were measured in the same-view membrane cell under a humid N_2 atmosphere. The aging (activated) MEA Pt/C sample (0 tri-ADT cycle) showed nearly homogeneous Pt distribution in the cathode layer (Figure 3 B), where there was few crack/hole (Figure 3 A and B). The valence of all Pt nanoparticles in the whole (B) and microscopic (G) areas was proved to be metallic by Pt valence maps in Figure 3 E and I and by nano-XANES spectra in Figure 3 L. However, the spatial distribution of ionomers was non-uniform as imaged in Figure 3 D. The Pt metallic state and its spatial uniformity were confirmed by nano-EXAFS analysis in the boundary areas with the polymer electrolyte (e in A) and GDL (g in A) and in the middle cathode area (m in A) as shown in Figure 3 M (nano-EXAFS oscillations) and N (nano-EXAFS Transforms), where only Pt-Pt bonds at 0.275 nm were observed and no Pt-O bonds were detected. The more detailed fitting results and structural parameters are shown in Figure S2 and Table S1 (supporting information). These results demonstrate the uniform distribution of metallic Pt^0 nanoparticles in the whole cathode region of the activated MEA Pt/C (0 tri-ADT cycle).

After 10 tri-ADT cycles (Figure 4), the cathode catalyst layer became thin compared to the images of Figure 3 as a result of carbon corrosion. However, the Pt valence kept in zero (Figure 4 E and I). In the boundary region of the cathode with the electrolyte, the size of carbon (Figure 2A) reduced and lots of Pt nanoparticles detached from the cathode carbon as imaged in Figure 4 F and J. We performed nano-XAFS measurements in the nano regions

including the detached Pt nanoparticles (d1 and d2 marked with red squares in Figure 4 F and J) and the edge areas of the cathode layer (e1 and e2 marked with red squares in Figure 4 F and J). The nano-XANES spectra for d1, d2, e1 and e2 areas are shown in Figure 4 M, which are all similar to the XANES for Pt metal foil. Nano-EXAFS data for the nano areas (d1, d2, e1 and e2) are shown in Figure 4 N and O, where the EXAFS oscillations and

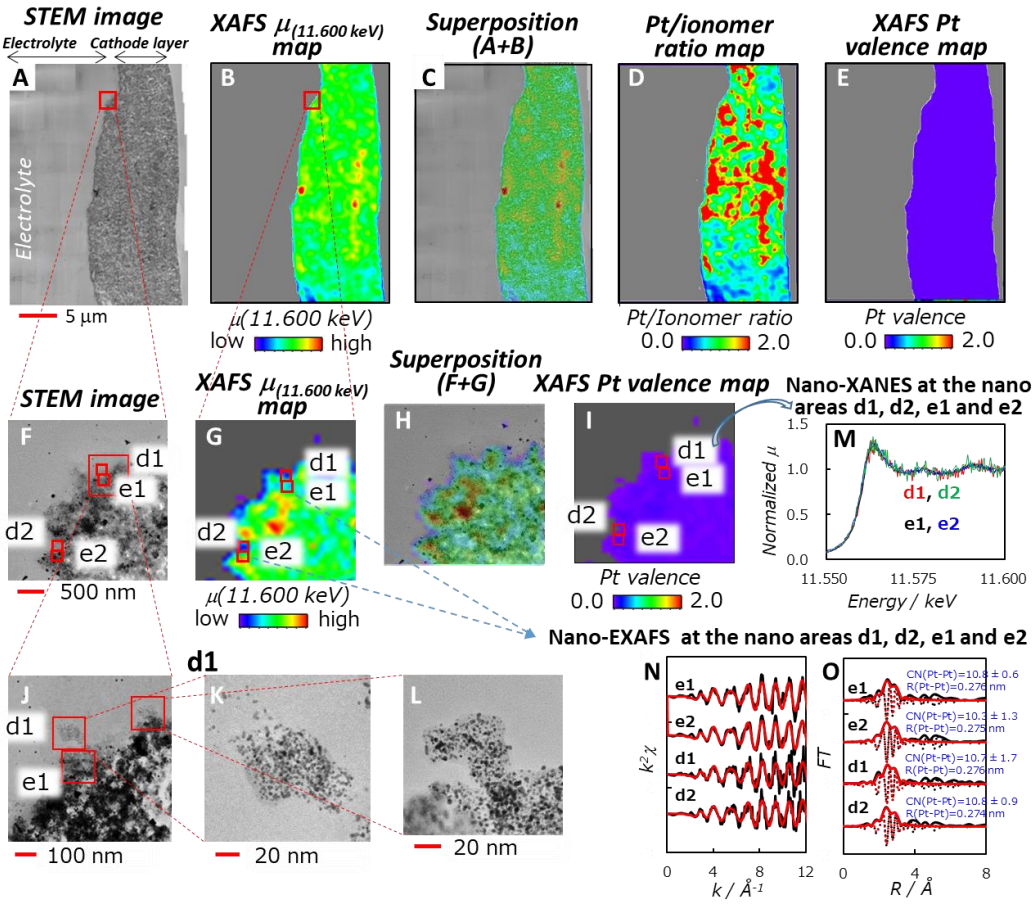

Figure 4. The same-view nano-XAFS/STEM-EDS imaging of the degraded MEA cathode electrocatalyst after 10 tri-ADT cycles for the 30 x 24 µm^2 (**A** - **E**) and 3 x 3 µm^2 regions (**F** - **I**). **A** and **F**: STEM images; **B** and **G**: XAFS absorbance $\mu_{(11.600\ keV)}$ map; **C** and **H**: the superpositions of **A** and **B** and **F** and **G**, respectively; **D**: map of Pt/Ionomer ratios; **E** and **I**: XAFS Pt valence maps; **J** - **L**: STEM images for the indicated red square areas; **M**: nano XANES for the nano-square regions **d1**(red), **d2** (green), **e1**(black) and **e2**(blue) shown in **F**, **G**, **I** and **J**. **N** and **O**: nano-EXAFS oscillations (**N**) and Fourier transforms (**O**) and their fittings (red); CN(Pt-Pt) and R(Pt-Pt) are shown in **O** (see Figure S3 and Table S2). The beam sizes are 210 x 226 nm and 142 x 159 nm for **B** - **E** and **G** – **I**, respectively.

Fourier transforms are presented with fitting curves (red). The detailed fitting data and determined structural parameters are shown in Figure S3 and Table S2 (SI). In every nano region of the MEA Pt/C sample after the 10 tri-ADT cycles only Pt-Pt bonds around 0.275 nm were observed and no Pt-O bonds were observed. The results on the Pt valence maps for the cathode layer and the detailed EXAFS analysis for the nano areas evidence that both detached Pt nanoparticles and edge area-located Pt nanoparticles at the initial stage of MEA degradation are still metallic. Thus, it is concluded that the Pt detachment occurred without any change/oxidation of Pt chemical species in the early degradation stage of MEA Pt/C.

After 20 tri-ADT cycles, the cathode catalyst layer became thinner and definite cracks and holes were formed as a result of carbon corrosion as shown in the STEM image of Figure 5 A under a humid N_2 atmosphere. The Pt distribution became heterogeneous clearly after the 20 tri-ADT cycles as depicted by the XAFS map in Figure 5 B. The ionomer concentration was also heterogeneous (Figure 5 D). Figure 5 E and I revealed the Pt valence map, where the location of Pt oxidized species was visualized only in the boundary region with the electrolyte and also in the cracks and holes. In the 20 tri-ADT sample we found remarkably degraded areas in the boundary region, where the size of carbon nanoparticles reduced to ~8 nm (Figure 5 F, J and K). On such carbons most of Pt nanoparticles detached and aggregated as shown in Figure 5 F, J and K. Then, we performed same-view nano-XAFS measurements to estimate Pt chemical species in the corroded carbon areas c1 and c2 in Figure 5. Also, as a reference, a nano area n1 (Figure 5 F and L) with a normal size of carbon was measured. The Pt distribution map and Pt valence map are shown in Figure 5 G and I, where the beam size (nano-XAFS measurement area) was as small as 142 x 159 nm^2. The normalized XANES spectra for the nano areas c1, c2, and n1 are shown in Figure 5 M. The white line peak intensity for the c1 and c2 areas was larger than that for the n1

area. The Pt valences in the c1 and c2 areas were estimated as 0.4 ±0.05, while the Pt valence in the n1 area was zero. The nano-EXAFS analysis results for the c1, c2 and n1 areas in Figure 5 G are shown in Figure 5 N (oscillations) and O (Fourier transforms). The detailed fitting data and determined structural parameters are shown in Figure S4 and Table S3 (SI). In these corroded carbon areas (c1 and c2) the coordination numbers of Pt-Pt bonds

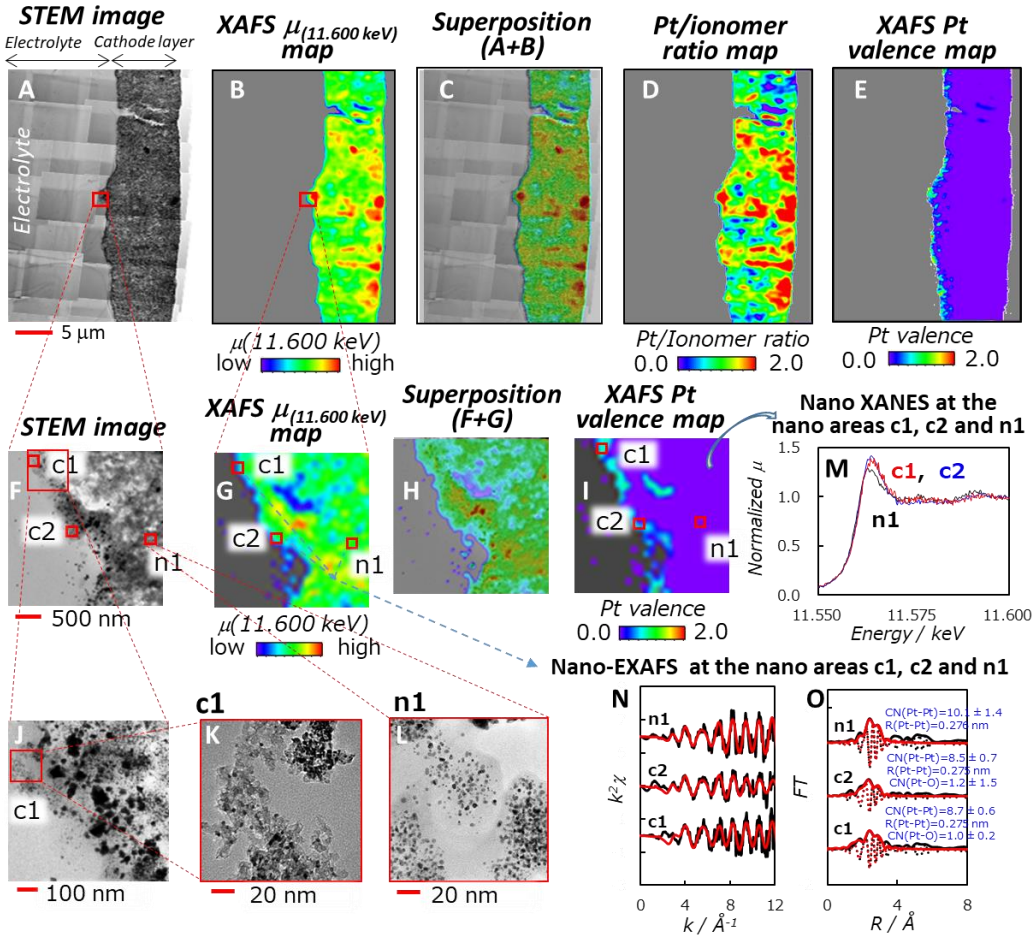

Figure 5. The same-view nano-XAFS/STEM-EDS imaging of the degraded MEA cathode electrocatalyst after 20 tri-ADT cycles for the 40 x 24 µm (**A** - **E**) and 3 x 3 µm regions (**F** - **I**). **A** and **F**: STEM images; **B** and **G**: XAFS absorbance $\mu_{(11.600\ keV)}$ map; **C** and **H**: the superpositions of **A** and **B** and **F** and **G**, respectively; **D**: map of Pt/Ionomer ratios; **E** and **I**: XAFS Pt valence maps; **J**- **L**: STEM images for the indicated red square areas; **M**: nano-XANES for the regions **c1**(red), **c2** (blue) and **n1** (black) shown in **F**, **I** and **J**. **N** and **O**: nano-EXAFS oscillations (**N**) and Fourier transforms (**O**) and their fittings (red); CN(Pt-Pt), R(Pt-Pt) and CN(Pt-O) are shown in **O** (see Figure S4 and Table S3). The beam sizes are 210 x 226 nm and 142 x 159 nm for **B** - **E** and **G** – **I**, respectively.

(CN_{Pt-Pt}) were 8.7 and 8.5, respectively, which are smaller than the CN_{Pt-Pt} (10.1) for the n1 area that is similar to the value (10.8) estimated from the averaged Pt nanoparticle size (~2.8 nm) for the aging Pt/C sample (Figure 2).[30,31] The coordination numbers of Pt-O bonds (CN_{Pt-O}) in the c1 and c2 areas were determined to be 1.0 and 1.2, respectively (Table S3). These XANES and EXAFS results for the 20 tri-ADT sample reveal that oxidized Pt species were formed and remained in the areas around small corroded carbon supports (~8 nm) in the boundary region with the electrolyte layer. On the other hand, no Pt-O bonds (CN_{Pt-O} =0) were observed in the n1 area, which agrees with the Pt valence analysis (Figure 5 M).

Previously, we reported the formation of Pt^{2+}-O_4 with a four coordination structure in the large μm-crack region by rectangular-wave 0.6-1.0 V_{RHE} ADT (rec-ADT) cycles on the basis of the Pt valence estimated by the nano-XANES and the CN_{Pt-O} estimated by the nano-EXAFS.[29-31] The white line intensities of the normalized XANES spectra for Pt foil, $Pt(acac)_2$, PtO and PtO_2 are regarded to be proportional to their Pt valences.[16] The XANES spectra for the degraded MEA Pt/C electrocatalysts were well fitted by a linear combination of Pt foil XANES and PtO XANES.[16, 29-31] There existed an isosbestic point at 11,569.7 eV in the nano-XANES spectra during the course of rec-ADT cycles, which suggested a direct transformation of Pt^0 to Pt^{2+} species without any stable intermediate states in the rec-ADT durability test operation. Figure 6 shows a series of nano-XANES spectra for the MEA Pt/C samples after the aging (0 tri-ADT), 10, 20 and 50 tri-ADT (1.0–1.5 V_{RHE}) cycles in the present study, which also revealed the existence of an isosbestic point at 11,569 eV. Previously, the Pt oxidation states of +2.0 (±0.1) valences were also observed in micro cracks/holes of Pt/C cathodes in degraded MEAs, where the CNs of Pt-O were about 4.0 (±0.4) and no Pt-Pt bonding was observed and neither nano size nor sub-nano size particles

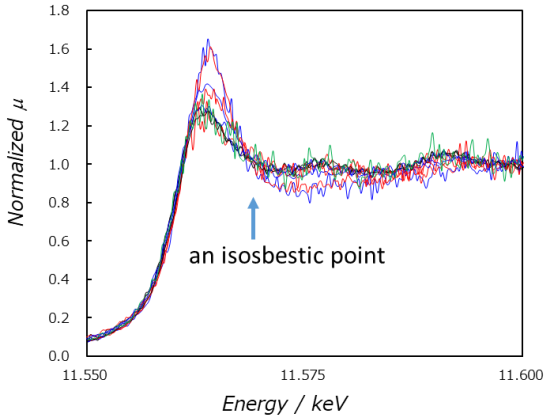

Figure 6. The existence of an isosbestic point in a series of nano-XANES spectra for the MEA Pt/C samples after the aging (0 tri-ADT), 10, 20 and 50 tri-ADT cycles.

Table 1. The molar fractions of Pt^0 and Pt^{2+}-O_4 species estimated from Pt valence, CN_{Pt-Pt} and CN_{Pt-O} under the assumption that Pt species consists of only metallic Pt^0 nanoparticles and Pt^{2+}-O_4 species with a four coordination structure in the regions of **c1**, **c2** and **n1** in Figure 5 for the MEA Pt/C after 20 tri-ADT cycles and **b1**, **b2** and **N1** and **I**, **II** and **III** in Figure 7 for the MEA Pt/C after 50 tri-ADT cycles.

Nano areas	from Pt valence		from CN_{Pt-Pt}		from CN_{Pt-O}	
	Pt^0(%)	Pt^{2+}-O_4(%)	Pt^0(%)	Pt^{2+}-O_4(%)	Pt^0(%)	Pt^{2+}-O_4(%)
20 tri-ADT sample						
c1	80	20	80	20	70	30
c2	80	20	80	20	70	30
n1	100	0	100	0	100	0
50 tri-ADT sample						
b1	30	70	40	60	40	60
b2	40	60	40	60	40	60
N1	100	0	100	0	100	0
I	30	70	20	80	40	60
II	40	60	20	80	40	60
III	100	0	100	0	100	0

were observed by the highest magnification 1,500,000 of TEM.[29,30] These results suggest Pt^{2+}-O_4 monomeric species.[29] In other degraded MEA Pt/C cathodes treated by anode gas exchange cycles we also observed monomeric Pt^{2+} species (Pt valence: +1.9 (±0.15)) with only Pt-O bonds and the CN_{Pt-O} of 2.3 (±0.8) at 0.211 nm (±0.007 nm).[30] The bond distance and coordination number of Pt-O indicate monomeric $Pt(OH)_2$ species. Assuming four

coordination, the $Pt(OH)_2$ may be loosely coordinated with water and the Nafion ionomer (Nf-SO_3 groups) in equilibrium; e.g. $[Pt(OH)_2(Nf\text{-}SO_3)_x(H_2O)_y]$.[29-31]

Thus, following the previous findings and discussion and assuming that Pt species consist of metallic Pt^0 nanoparticles and Pt^{2+}-O_4 species in the nano areas c1, c2 and n1 in the boundary region (Figure 5 G), we estimated the molar fractions of Pt^0 nanoparticles and Pt^{2+}-O_4 species in c1, c2 and n1 areas from the white line intensity (Pt valence) and the $CN_{Pt\text{-}Pt}$ and $CN_{Pt\text{-}O}$ as listed in Table 1. A part of Pt nanoparticles was oxidized in the c1 and c2 areas around the degraded carbon with smaller sizes than ~8 nm, whereas in the n1 area nearly all Pt nanoparticles remained metallic. The estimated molar fractions of Pt^{2+}-O_4 species for the c1 and c2 areas were 20–30% from the parameters, Pt valence, $CN_{Pt\text{-}Pt}$ and $CN_{Pt\text{-}O}$ (Table 1). The fractions estimated from the XANES Pt valence and the EXAFS CNs were similar to each other, which suggests that the majority of the oxidized Pt species is assigned to the Pt^{2+}-O_4 species with a four coordination structure and the Pt^{2+}-O_4 species coexist with metallic Pt^0 nanoparticles (70–80% fraction) in the nano areas c1 and c2.

After 50 tri-ADT cycles, the thickness of the cathode catalyst layer reduced by 40% (Figure 7 A–C). The Pt distribution became more heterogeneous after 50 tri-ADT cycles (Figure 7 B). Figure 7 E and I show the Pt valence map and location of the Pt oxidized species in the boundary region with the electrolyte and also in the cracks and holes. In the 50 tri-ADT sample, interestingly, we observed an appearance of unusual carbon region with carbon sizes below 8 nm in dimension across over a wide range of the boundary of the cathode catalyst layer with the electrolyte (b1 and b2 in Figure 7 F). In this region, the initial morphology of the carbon support was lost and became flat. Moreover, only non-oriented graphite structures were observed by TEM (Figure 7 F, J and K) though the non-degraded carbon support (Ketjenblack) possessed an oriented longer stacking graphite

structure. The above carbon region with the non-orientated graphite structure might have been formed by an aggregation of very small corroded carbons (below a few nm). The normalized XANES spectra for the nano areas b1 and b2 marked with red squares in Figure 7 F, I and J showed the larger white line peak intensity than that for the N1 area with

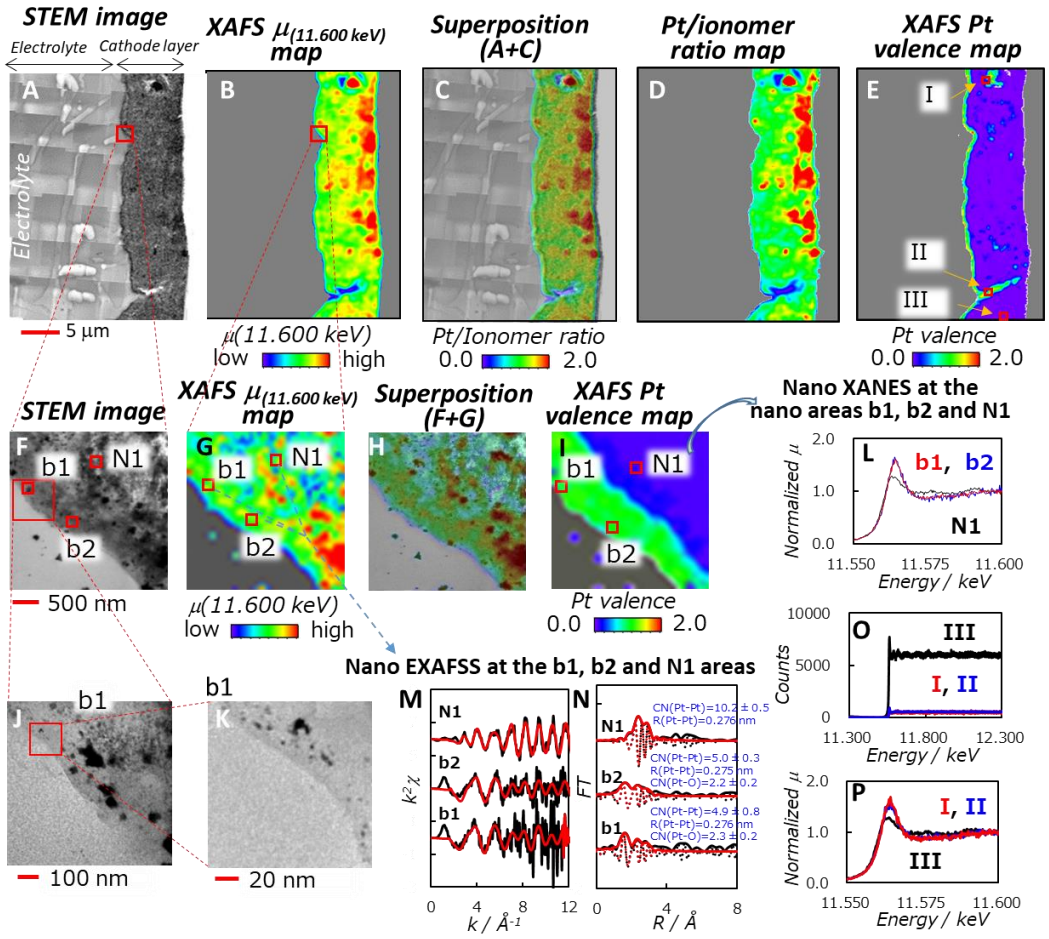

Figure 7. The same-view nano-XAFS/STEM-EDS imaging of the degraded MEA cathode electrocatalyst after 50 tri-ADT cycles for the 34 x 24 μm (**A** - **E**) and 3 x 3 μm regions (**F** - **I**). **A** and **F**: STEM images; **B** and **G**: XAFS absorbance $\mu_{(11.600\ keV)}$ map; **C** and **H**: the superpositions of **A** and **B** and **F** and **G**, respectively; **D**: map of Pt/Ionomer ratios; **E** and **I**: XAFS Pt valence maps; **J** and **K**: STEM images for the indicated red square areas; **L**: nano XANES for the regions **b1**(red), **b2** (blue), **N1** (black) shown in **F**, **G** and **I**. **M** and **N**: nano-EXAFS oscillations (**M**) and Fourier transforms (**N**) and their fittings (red); CN(Pt-Pt), R(Pt-Pt) and CN(Pt-O) are shown in **N** (see Figure S5 and Table S4). **O**: Nano-XAFS spectra; **P**: nano-XANES spectra, in the nano regions I, II and III for the 50 tri-ADT sample in Figure 7 **E**. The beam sizes are 210 x 226 nm and 142 x 159 nm for **B** - **E** and **G** – **I**, respectively

metallic Pt^0 nanoparticles (Figure 7 L). Figure 7 L and Figure 6 for the series of nano-XANES spectra reveal an isosbestic point at 11,569 eV, indicating the direct transformation of Pt^0 to Pt^{2+} during the 50 tri-ADT degradation. The estimated molar fractions of Pt^0 nanoparticles and Pt^{2+}-O_4 species in b1, b2 and N1 are also listed in Table 1. The fractions of the Pt^{2+}-O_4 species in b1 and b2 were 60–70%, while the fractions of metallic Pt^0 nanoparticles were 30–40%. In the N1 area metallic Pt^0 nanoparticles remained unchanged (100% fraction), where no Pt^{2+} ions were observed. The nano-EXAFS analysis results for the b1, b2 and N1 areas marked with red squares in Figure 7 F and G are shown in Figure 7 M (oscillations) and N (Fourier transforms). The size of the measured nano-regions was 142 nm x 159 nm (same as the beam size). The detailed fitting data and determined structural parameters are shown in Figure S5 and Table S4 (SI). In these corroded carbon areas (b1 and b2) the $CN_{Pt\text{-}Pt}$ values were 4.9 and 5.0, respectively, which are much smaller than the $CN_{Pt\text{-}Pt}$ (10.2) for the N1 area. The $CN_{Pt\text{-}O}$ values in the b1 and b2 areas were determined to be 2.2–2.3, which are 1.8–2.3 times larger than those for the c1 and c2 areas in the 20 tri-ADT sample. No Pt-O bonds were observed in the N1 area. The same-view nano-XAFS/STEM-EDS technique for the 50 tri-ADT sample evidences that the Pt oxidation is more pronounced in the extremely corroded region of carbon support.

Figure 7 O and P show the nano-XANES spectra for the hole and crack regions (I and II, respectively in Figure 7 E) and non-degraded region (III in Figure 7 E), and the nano-EXAFS data for the regions I–III and structural parameters determined by the curve fitting analysis are shown in Figure S6 and Table S5 (SI). It was found that the averaged Pt valence for Pt species in the hole/crack regions (I and II) reached to 1.4+ and 1.2+, respectively (Table 1). In the non-degraded carbon region (III) the Pt valence was zero. The molar fractions of Pt^0 and Pt^{2+}-O_4 species in these regions were also calculated by the Pt valence,

CN(Pt-Pt) and CN(Pt-O) as listed in Table 1. The fractions of the Pt^{2+}-O_4 species in both hole and crack regions were 60–80% (Table 1). Hence, the Pt^{2+}-O_4 fractions in the I and II areas correspond to an averaged Pt valence around 1.4+, which agrees with the above estimated Pt valence around 1.3+ within experimental error bars. Thus, it is suggested that the majority of Pt species in the crack/hole region after the 50 tri-ADT cycles is Pt^{2+}-O_4 species. The Pt nanoparticles were oxidized in the crack/hole regions (I and II) similar to the boundary regions (b1 and b2) with the electrolyte layer, even more oxidized in the crack/hole nano areas (I and II) than in the nano areas (b1 and b2) of the boundary region. The CN(Pt-Pt) values were 2.5–2.7 (Table S5), which are smaller than the values 4.9 and 5.0 for the b1 and b2 areas in the boundary region with the electrolyte. This result also indicates more deterioration of Pt nanoparticles to Pt^{2+} ions accompanied with Pt-Pt dissociation in the crack/hole regions. We estimated the amount (density) of the Pt species, which are detached as Pt^0 nanoparticles and dissolved as Pt^{2+}-O_4 species, in the nano areas I and II from the nano-XAFS spectra in Figure 7 O and Figure S6 O. The amounts of the total Pt species in the nano areas I (hole) and II (crack) were 7% and 8% of that in the III (no deterioration) area.

Figure 8 shows the effects of crack/hole size and Pt/ionomer ratio on Pt valence in the 0–50 tri-ADT samples. The relationships between Pt valence (red) and crack/hole size and between crack/hole number (blue) and crack/hole size are illustrated in Figure 8 A, and the relationships between Pt valence (red) and Pt/ionomer ratio and between crack/hole number (blue) and Pt/ionomer ratio are illustrated in Figure 8 B. The number of cracks and holes in the MEA Pt/C cathode layer increased with increasing tri-ADT cycles along with corrosion of the carbon support becoming thinner, where the Pt/ionomer ratio increased in the cracks/holes, particularly less than ~700 nm. The Pt valence was more positively

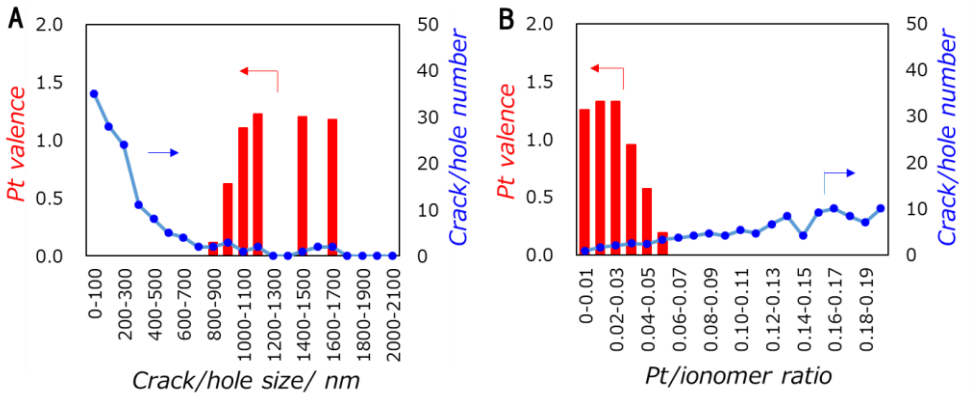

Figure 8. Effects of crack/hole size and Pt/ionomer ratio on Pt valence in the 0–50 tri-ADT samples. ***A***: The relationships between Pt valence (red) and crack/hole size and between crack/hole number (blue) and crack/hole size. ***B***: The relationships between Pt valence (red) and Pt/ionomer ratio and between crack/hole number (blue) and Pt/ionomer ratio.

charged in the larger crack/hole sizes than ~800 nm and in the crack/hole areas with the Pt/ionomer ratios below ~0.06. In such crack/hole regions the detached Pt^0 nanoparticles (30–40% fraction) and dissolved Pt^{2+}-O_4 species (60–70% fraction) coexist. Recently, we observed the similar tendency with the MEA Pt/C sample after 5,000 rect-ADT (0.6-1.0 V_{RHE}) cycles.[31] The degradation tendency in the crack/holes areas under the rect-ADT and tri-ADT protocols is suggested to be similar though the intense carbon corrosion under the 50 tri-ADT treatment above mentioned was not observed under the 5,000 rect-ADT treatment.

The same-view nano-XAFS and TEM/STEM-EDS measurement technique enabled us, for the first time, to directly visualize and analyze the degradation process of both carbon and Pt species involving supported Pt^0 metallic nanoparticles, detached Pt^0 metallic nanoparticles and dissolved Pt^{2+} oxidized species in the MEA Pt/C cathode electrocatalyst layer during the 0–50 tri-ADT operations, which is illustrated in Scheme 2. The application of the tri-ADT cycles caused at first the carbon corrosion and deterioration to reduce carbon size and to make carbon layer thin, particularly in the boundary region with the electrolyte

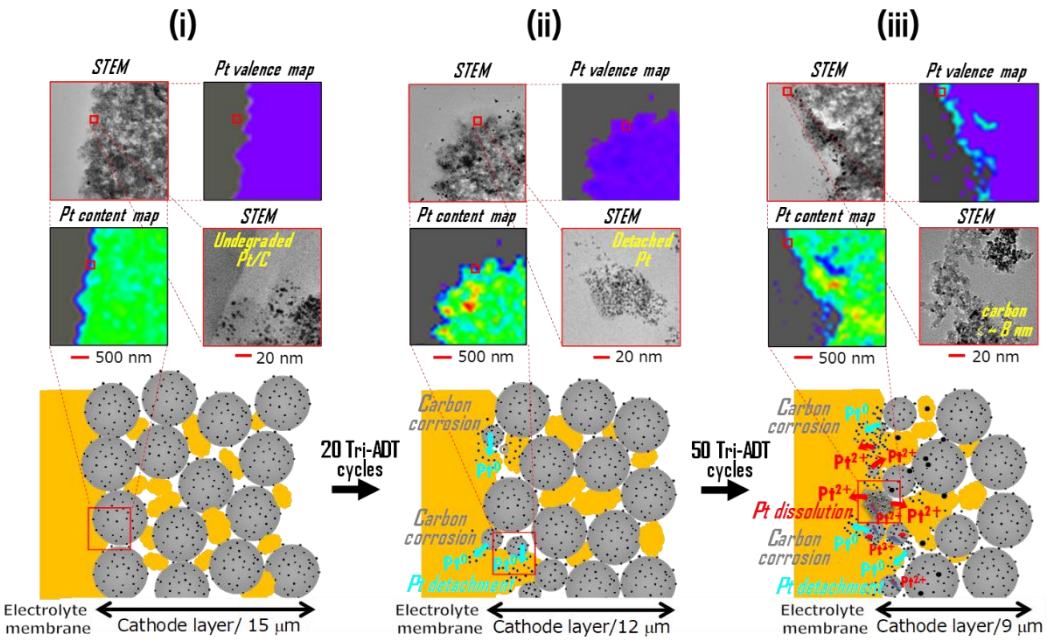

Scheme 2. Visualized schematic diagram for the degradations of carbon support and Pt nanoparticles in MEA Pt/C cathode electrocatalyst layer under the triangular-wave ADT (startup/shutdown) cycles. (Stage i) the initial Pt/C cathode electrocatalyst in MEA after aging (activating) treatment, (Stage ii) the degradation of the MEA Pt/C cathode in the boundary region with the electrolyte, where carbon corrosion caused decreases in the carbon size and cathode layer, accompanied with the detachment of Pt nanoparticles, and (Stage iii) the degradations in the cathode areas around extremely corroded carbon and in the cracks/holes in the boundary region with the electrolyte, where carbon size decreased to below ~8 nm and Pt^0 nanoparticles were oxidized and dissolved into Pt^{2+}-O_4 species in addition to the detachment.

(stage i), which was accompanied with the detachment of metallic Pt^0 nanoparticles (stage ii). Then, after the cathode carbon size decreased to less than ~ 8 nm, Pt^0 nanoparticles in the extremely corroded carbon region were oxidized and dissolved into Pt^{2+}-O_4 species in the interface areas and cracks/holes depending on the crack/hole size and Pt/ionomer ratio (stage iii).

Conclusions

We achieved the first success in the direct observation of the degradation process in the

MEA Pt/C cathode layer caused by the 1.0–1.5 V_{RHE} triangular-wave accelerated degradation test (tri-ADT) treatments (startup/shutdown operations) by the same-view nano-XAFS/STEM-EDS technique using the SiN membrane stacking cell under a humid N_2 atmosphere. The site-preferential areas, sequence and relationship of the degradations of carbon support and Pt nanoparticles in the boundary regions of the cathode electrocatalyst layer with the electrolyte and cracks/holes and also in the cracks/holes were visualized and analyzed by the same-view nano-XAFS/STEM-EDS method. By increasing tri-ADT cycles and after 20 tri-ADT cycles, carbon corrosion occurred more and the size of carbon nanoparticles decreased in the boundary regions. In the same regions, the detachment of supported Pt^0 nanoparticles without any chemical changes of Pt species was also observed. After 50 tri-ADT cycles the carbon size decreased to smaller sizes than ~8 nm to form the unusual boundary region. The fractions 60–70% and 60–80% of Pt^0 nanoparticles in the interface region around the extremely corroded carbons and in the produced cracks/holes, respectively were oxidized and dissolved into Pt^{2+}-O_4 species with a four coordination structure. The Pt degradation tendency in the cracks/holes was similar in the rect-ADT and tri-ADT protocols, where the Pt oxidation depended on the crack/hole size and Pt/ionomer ratio.

.

Experimental section.

MEA Pt/C samples. We purchased special MEAs with flat cathode/anode surface layer with few cracks/holes from EIWA FC Development Co, Ltd. Anode and cathode electrocatalysts were 50 wt% Pt/C (TKK, TEC10E50E). The Pt loadings for the anode and cathode electrocatalysts were 0.3 mg-Pt/cm^2. Pt/ionomer ratio was 1/1.

Electrochemical procedures. We applied 150 aging cycles for activation, and then

measured cyclic voltammetry (CV, 20 mV s^{-1}, and 50 mV s^{-1}) under anode/cathode=H_2/N_2. The degradation of MEA Pt/C samples was conducted by triangular-wave accelerated degradation test (tri-ADT) cycles between 1.0 and 1.5 V_{RHE}. In this study the MEA Pt/C sample after aging (0 tri-ADT cycle) was treated by 10, 20 and 50 tri-ADT cycles. Between each tri-ADT cycle, CVs under anode/cathode = H_2/N_2 and IV polarization curves under anode/cathode = H_2/Air were measured to check the degradation level of the MEA Pt/C samples. After all electrochemical procedures the anode/cathode gas was changed to N_2/N_2 and left until the cell potential reached circuit voltage (OCV) to avoid undesired oxidation of the MEA Pt/C. Then the MEA was taken from the electrochemical cell under a humid N_2 atmosphere.

Preparations of sliced MEA pieces for the same-view nano-XAFS and TEM/STEM-EDS observations. Sliced MEA samples for the same-view nano XAFS and TEM/STEM-EDS were prepared after 0, 10, 20 and 50 tri-ADT cycles treatments of the purchased MEA Pt/C using the similar method to that in our previous report.[29] The MEAs were sliced to 200 nm-thick and placed on a SiN membrane in 100 nm-thick under humid N_2 atmosphere as illustrated in Figure 1 A. The SiN membrane was sandwiched with another SiN membrane at a distance of 300 nm. All procedures during the preparation were performed under humid N_2 atmosphere. The same-view nano-XAFS and TEM/STEM-EDS measurements were conducted in a SiN stacking membrane cell in Figure 1 A. Thus, the same-view measurements are regarded to be equivalent to in situ observations due to slow irreversible phenomenon of the MEA degradation.

Same-view nano-XAFS and TEM/STEM-EDS measurements. Same-view nano-XAFS and TEM/STEM-EDS measurements were performed in a similar way to that described in our previous report.[30] By using the SiN membrane stacking cell containing the sliced MEA

piece sample, at first TEM/STEM-EDS of an MEA Pt/C sample in the membrane cell under humid N_2 atmosphere was measured on a JEM-2100F equipped with an energy dispersive spectrometer (EDS) at 200 kV. STEM-EDS images were observed by electron beams with 0.7 nm of spot size. Pt nanoparticles move on the support carbon in TEM/STEM-EDS observations under the humid N_2 atmosphere without any temperature control though Pt migrations are never observed with dried MEA samples under high vacuum.[30] To avoid the formation of bubbles by water boiling in the specimen and the moving and aggregation of Pt nanoparticles during the TEM/STEM observations under the humid N_2 atmosphere, the sample temperature was regulated at 300.5 K by a Cryo-holder, at which temperature Pt nanoparticles neither moved nor aggregated. The TEM/STEM observations were performed for 2~3 views of 80 x 20 μm^2 regions for each MEA piece sample. Then, nano-XAFS spectra for the same MEA piece sample in the SiN membrande cell under humid N_2 atmosphere were measured. For the position calibration of nano-XAFS map and STEM image we used the orthogonal distance regression for the estimation of fitting parameters p_0, p_1 and p_2 to give a minimum residual; $A(x,y) - p_0 * B(x-p_1,y-p_2)$ ($A(x,y)$: absorbance of nano-XAFS map and $B(x,y)$: contrast of the STEM image for coordinate point (x,y)). Thus, the positions were calibrated by using the calculated p_1 and p_2.[30]

The Pt L_{III}-edge nano-XAFS spectra were measured at BL36XU by using a Si(111) double crystal monochromator. X-ray beam (11.390–12.160 keV) was focused to 210 nm x 226 nm size or 142 nm x 159 nm size via a pair of elliptically bent Kirkpatrick-Baez (KB) mirrors. The nano-XAFS spectra were measured in a fluorescence mode using a 25-element Ge detector (CANBERRA), where the sample was inclined to the X-ray nanobeam by 30º. In the scanning nano-XAFS method, a XAFS spectrum was obtained from 206 energy points (a total of 206 maps). During the repeated nano-XAFS measurements (20 min

acquisition), there were no significant changes in the nano-XANES, but after totally 25 min acquisition the nano XRF map changed and the edge jump dropped. Thus, it is indicated that nano-X-ray beam irradiation damage for the nano-XAFS measurement can be neglected till 20 min acquisition. To avoid a sample damage, a beam stay time in a pixel point was shortened as much as possible. Nano-XAFS mapping was performed for 1–2 views of about 30 x 25 μm^2 and 1 view of 3 x 3 μm^2 using nano X-ray beam with 210 x 226 nm^2 and 142 x 159 nm^2 size every 400 nm and 200 nm-step, respectively. Beam stay time at the same nano position for nano-XAFS maps in about 30 x 25 μm^2 and 3 x 3 μm^2 regions was only 100 ms and 200 ms, respectively. For nano-XAFS measurements, we also performed 60 s x 10 loops and 300 s x 10 loops measurements for nano spots, 210 x 226 nm^2 and 142 x 159 nm, respectively.

Analysis of XAFS data. Data analyses, XANES fitting, and EXAFS Fourier transform fitting were performed similar to the previous reports.[15,30] The spectra were treated by using the data analysis program IFEFFIT (version 1.2.11c).[35] Theoretical phase shift and backscattering amplitude functions were calculated from the program FEFF 8.20.[36] Normalized white line peak areas for estimation of Pt valences were calculated by using Lorentzian and Arctangent functions by IFEFFIT. We used s_0^2 values of 0.88 and 0.90 in the determination of $CN_{Pt\text{-}Pt}$ and $CN_{Pt\text{-}O}$, respectively. The FT window taken in the $k^2\chi$ plots and the fitting range in R space were 3-11 $Å^{-1}$ and 1.4-3.2 Å, respectively. To avoid divergence in the XANES fitting analysis of the XANES mapping regions, we ignored low Pt contents below 1/100 of $\mu_{11.600}$ keV.

Analysis on the distribution of particle sizes of Pt nano particle and carbon support. The sizes of Pt nanoparticle and carbon support in 80 μm regions were averaged. The boundary regions with the electrolyte, crack/holes and gas diffusion layer (GDL) were defined as 100

nm-wide regions of the cathode catalyst layer from the boundary end.

Supporting Information. Same-view membrane cell; nano-XANES spectra; nano-EXAFS data and analysis; structural parameters of Pt species. This material is available free of charge via the Internet http://pubs.acs.org.

AUTHOR INFORMATION

Corresponding Author

* Yasuhiro Iwasawa

Tel: +81-42-443-5921; Fax: +81-42-443-5483

E-mail: iwasawa@pc.uec.ac.jp

Author Contributions

The manuscript was written through contributions of all authors. All authors have given approval to the final version of the manuscript.

Conflict of Interest

The authors declare no competing financial.

ACKNOWLEDGMENT

This work was supported by the New Energy and Industrial Technology Development Organization (NEDO). XAFS measurements were performed with the approval of SPring-8 subject numbers 2013A7803, 2013B7803, 2014A7806, 2014B7804, 2015A7804, 2015B7804, 2016A7804, 2016B7804, and 2017A7804.

References

(1) Zhao, X.; Takao, S.: Higashi, K.; Kaneko, T.; Samjeskè, G.; Sekizawa, O.; Sakata, T.; Yoshida, Y.; Uruga, T.; Iwasawa, Y. Simultaneous Improvements of Performance and Durability of an Octahedral $PtNi_x$/C Electrocatalyst for Next–Generation Fuel Cells by Continuous, Compressive and Concave Pt Skin Layers. *ACS Catal.* **2017**, *7*, 4642–4654.

(2) Ellingsen, L. A.-W.; Hung, C. R.; Singh G. M.-B. B.; Chen, Z.; Whittingham, M. S.; Strømman, A. H. Nanotechnology for Environmentally Sustainable Electromobility. *Nat. Nanotechnol*. **2016**, *11*, 1039-1051.

(3) Schmidt, O.; Hawkes, A.; Gambhir, A.; Staffell, I. The Future Cost of Electrical Energy Storage Based on Experience Rates. *Nat. Energy* **2017**, *2*, 17110-1-8.

(4) Costentin, C.; Savéant, J. M. Towards an Intelligent Design of Molecular Electrocatalysts. *Nat. Rev. Chem.* **2017**, *1*, 0087-1-8.

(5) Dey, S.; Mondal, B.; Chatterjee, S.; Rana, A.; Amanullah, S.; Dey, A. Molecular Electrocatalysts for the Oxygen Reduction Reaction. *Nat. Rev. Chem.* **2017**, *1*, 0098-1-20.

(6) https://energy.gov/eere/fuelcells/doe-technical-targets-polymer-electrolyte-membrane-fuel-cell-components.

(7) Chen, S.; Wei, Z.; Qi, XQ.; Dong, L.; Guo, Y.-G. Wan, L.; Shao, Z.; Li, L. Nanostructured Polyaniline-Decorated Pt/C@PANI Core−Shell Catalyst with Enhanced Durability and Activity. *J. Am. Chem. Soc*. **2012**, *134*, 13252−13255.

(8) Huang, S.-Y.; Ganesan, P.; Park, S.; Popov, B. N. Development of a Titanium Dioxide-Supported Platinum Catalyst with Ultrahigh Stability for Polymer Electrolyte Membrane Fuel Cell Applications. *J. Am. Chem. Soc*. **2009**, *131*, 13898–13899.

(9) Wu, Z. Lv, Y.; Xia, Y.; Webley, P. A.; Zhao, D. Ordered Mesoporous Latinum@Graphitic Carbon Embedded Nanophase as a Highly Active, Stable, and Methanol-Tolerant Oxygen Reduction Electrocatalyst. *J. Am. Chem. Soc*. **2012**, *134*, 2236−2245.

(10) Subban, C. V.; Zhou, Q.; Hu, A,; Moylan, T. E.; Wagner, F. T.; DiSalvo, F. J. Sol-Gel Synthesis, Electrochemical Characterization, and Stability Testing of $Ti_{0.7}W_{0.3}O_2$ Nanoparticles for Catalyst Support Applications in Proton-Exchange Membrane Fuel Cell. *J. Am. Chem. Soc*. **2010**, *132*, 17531–17536.

(11) Sui, S.; Wang, X.; Zhou, X.; Su, Y.; Riffat, S.; Liu, C. A Comprehensive Review of Pt Electrocatalysts for the Oxygen Reduction Reaction: Nanostructure, Activity, Mechanism and Carbon Support in PEM Fuel Cells. *J. Mater. Chem. A* **2017**, *5*, 1808−1825.

(12) Arenz, M.; Zana, A. Fuel Cell Catalyst Degradation: Identical Location Electron Microscopy and Related Methods. *Nano Energy* **2016** *29*, 299−313.

(13) Speder, J.; Zana, A.; Spanos, I.; Kirkensgaard, J. J. K.; Mortensen, K.; Hanzlik, M.; Arenz, M. Comparative Degradation Study of Carbon Supported Proton Exchange Membrane Fuel Cell Electrocatalysts – The Influence of the Platinum to Carbon Ratio on the Degradation Rate. *J. Power Sources* **2014**, *261*, 14−22.

(14) Castanheria, L.; Silva, W. O., Lima, F. H. B.; Crisci, A.; Dubau, L.; Maillard, F. Carbon Corrosion in Proton-Exchange Membrane Fuel Cells: Effects of the Carbon Structure, the Degradation Protocol, and the Gas Atmosphere. *ACS Catal.* **2015**, *5*, 2184−2194.

(15) Iwasawa, Y., Asakura, K., Tada, M., Eds., XAFS Techniques for Catalysts, Nanomaterials, and Surfaces, Springer, 2017.

(16) Nagasawa, K.; Takao, S.; Higashi, K.; Nagamatsu, S.; Samjeské, G.; Imaizumi, Y.; Sekizawa, O.; Yamamoto, T.; Uruga, T.; Iwasawa, Y.; Performance and Durability of Pt/C Cathode Catalysts with Different Kinds of Carbons for Polymer Electrolyte Fuel Cells Characterized by Electrochemical and *In-situ* XAFS Techniques. *Phys. Chem. Chem. Phys.* **2014**, *16*, 10075-10087.

(17) Nagamatsu, S.; Arai, T.; Yamamoto, M.; Ohkura, T.; Oyanagi, H.; Ishizaka, T.; Kawanami, H.; Uruga, T.; Tada, M.; Iwasawa, Y. Potential-Dependent Restructuring and Hysteresis in the Structural and Electronic Transformations of Pt/C, Au(Core)-Pt(Shell)/C, and Pd(Core)-Pt(Shell)/C Cathode Catalysts in Polymer Electrolyte Fuel Cells Characterized by In Situ X-ray Absorption Fine Structure. *J. Phys. Chem. C* **2013**, *117*, 13094−13107.

(18) Nagamatsu, S.; Takao, S.; Samjeské, G.; Nagasawa, K.; Sekizawa, O.: Kaneko, T.; Higashi, K.; Uruga, T.; Gayen, S.; Velaga, S.; Saniyal, M. K.; Iwasawa, Y. Structural and Electronic Transformations of Pt/C, Pd@Pt(1 ML)/C and Pd@Pt(2 ML)/C Cathode Catalysts in Polymer Electrolyte Fuel Cells during Potential-Step Operating Processes Characterized by In-Situ Time-Resolved XAFS. *Surf. Sci*. **2016**, *648*, 100−113.

(19) Tada, M.; Murata, S.; Asaoka, T.; Hiroshima, K.; Okumura, K.; Tanida, H.; Uruga, T.; Nakanishi, H.; Matsumoto, S.; Inada, Y.; Nomura, M.; Iwasawa, Y. In Situ Time-Resolved Dynamic Surface Events on the Pt/C Cathode in a Fuel Cell under Operando Conditions. *Angew. Chem. Int. Ed*. **2007**, *46*, 4310−4315.

(20) Ishiguro, N.; Saida, T.; Uruga, T.; Nagamatsu, S.; Sekizawa, O.; Nitta, K.; Yamamoto,

T.; Ohkoshi, S.; Yokoyama, T.; Tada, M. Operando Time-Resolved X-ray Absorption Fine Structure Study for Surface Events on a Pt_3Co/C Cathode Catalyst in a Polymer Electrolyte Fuel Cell during Voltage-Operating Processes. *ACS Catal.* **2012**, *2*, 1319−1330.

(21) Ishiguro, N.; Saida, T.; Uruga, T.; Sekizawa, O.; Nagasawa, K.: Nitta, K.; Yamamoto, T.; Ohkoshi, S.; Yokoyama, T.; Tada, M. Structural Kinetics of a Pt/C Cathode Catalyst with Practical Catalyst Loading in an MEA for PEFC Operating Conditions Studied by In Situ Time-Resolved XAFS. *Phys. Chem. Chem. Phys*. **2013**, *15*, 18827−18834.

(22) Ishiguro, N.; Kityakarn, S.; Sekizawa, O.; Uruga, T.; Sasabe, T.; Nagasawa, K.; Yokoyama, T.; Tada, M. Rate Enhancements in Structural Transformations of Pt–Co and Pt–Ni Bimetallic Cathode Catalysts in Polymer Electrolyte Fuel Cells Studied by In Situ Time-Resolved X-ray Absorption Fine Structure. *J. Phys. Chem. C* **2014**, *118*, 15874−15883.

(23) Tada, M.; Uruga, T.; Iwasawa, Y. Key Factors Affecting the Performance and Durability of Cathode Electrocatalysts in Polymer Electrolyte Fuel Cells Characterized by In Situ Real Time and Spatially Resolved XAFS Techniques. *Catal. Lett. (Silver Anniversary Special Issue)* **2015**, *145*, 58-70.

(24) Kaneko, T.; Samjeské, G.; Nagamatsu, S.; Higashi, K.; Sekizawa, O.; Takao, S.; Yamamoto, T.; Zhao, X.; Sakata, T.; Uruga, T.; Iwasawa, Y. Key Structural Kinetics for Carbon Effects on the Performance and Durability of Pt/Carbon Cathode Catalysts in Polymer Electrolyte Fuel Cells Characterized by In Situ Time-Resolved X-ray Absorption Fine Structure. *J. Phys. Chem. C* **2016**, *120*, 24250–24264.

(25) Higashi, K.; Samjeské, G.; Takao, S.; Kaneko, T.; Sekizawa, O.; Uruga, T.; Iwasawa,

Y. The Relationship between the Active Pt Fraction in a PEFC Pt/C Catalyst and the ECSA and Mass Activity during Start-Up/Shut-Down Degradation by In Situ Time-Resolved XAFS Technique. *J. Phys. Chem. C* **2017**, *121*, 22164–22177.

(26) Sekizawa, O.; Uruga, T.; Higashi, K.; Kaneko, T.; Yoshida, Y.; Sakata, T.; Iwasawa, Y. Simultaneous Operando Time-Resolved XAFS/XRD Measurements of a Pt/C Cathode Catalyst in Polymer Electrolyte Fuel Cell under Transient Potential Operations. *ACS Sus. Chem. Eng*. **2017**, *5*, 3631−3636.

(27) Saida, T.; Sekizawa, O.; Ishiguro, N.; Hoshino, M.; Uesugi, K.; Uruga, T.; Ohkoshi, S.; Yokoyama, T.; Tada, M. 4D Visualization of a Cathode Catalyst Layer in a Polymer Electrolyte Fuel Cell by 3D Laminography–XAFS. *Angew. Chem. Int. Ed*. **2012**, *124*, 10311–10314.

(28) Yamashita, Y.; Itami, S.; Takano, J.; Kakinuma, K.; Uchida, H.; Watanabe, M.; Iiyama, A.; Uchida M. Degradation Mechanisms of Carbon Supports under Hydrogen Passivation Startup and Shutdown Process for PEFCs. *J. Electrochem. Soc.* **2017**, *164,* F181–F187.

(29) Takao, S.; Sekizawa, O.; Nagamatsu, S.; Kaneko, T.; Yamamoto, T.; Samjeské, G.; Higashi, K.; Nagasawa, K.; Tsuji, T.; Suzuki, M.; Kawamura, N.; Mizumaki, M.; Uruga, T.; Iwasawa, Y. Mapping Platinum Species in Polymer Electrolyte Fuel Cells by Spatially Resolved XAFS Techniques. *Angew. Chem. Int. Ed*. **2014**, *53*, 14110–14114.

(30) Takao, S.; Sekizwa, O.; Samjeské, G.; Nagamatsu, S.; Kaneko, T.; Yamamoto, T.; Higashi, K.; Nagasawa, K.; Uruga, T.; Iwasawa, Y. Same-View Nano-XAFS/STEM-EDS Imagings of Pt Chemical Species in Pt/C Cathode Catalyst Layers of a Polymer Electrolyte Fuel Cell. *J. Phys. Chem. Lett*. **2015**, *6*, 2121−2126.

(31) Takao. S.; Sekizawa, O.; Samjeské, G.; Nagamatsu, S.; Kaneko, T.; Higashi, K.; Yamamoto, T.; Nagasawa, Zhao, X.; K.; Uruga, T.; Iwasawa, Y. Spatially Non-Uniform Degradation of Pt/C Cathode Catalysts in Polymer Electrolyte Fuel Cells Imaged by Combination of Nano XAFS and STEM-EDS Techniques. *Top. Catal*. **2016**, *59*, 1722–1731.

(32) Sekizawa, O.; Uruga, T.; Takagi, Y.; Nitta, K.; Kato, K.; Tanida, H; Uesugi, K.; Hoshino, M.; Ikenaga, E.; Takeshita, K.; Takahashi, S.; Sano, M.; Aoyagi, H.; Watanabe, A.; Nariyama, N.; Ohashi, H.; Yumoto, H.; Koyama, T.; Senba, Y.; Takeuchi, T.; Furukawa, Y.; Ohata, T.; Matsushita, T.; Ishizawa, Y.; Kudo, T.; Kimura, H.; Yamazaki, H.; Tanaka, T.; Bizen, T.; Seike, T.; Goto, S.; Ohno, H.; Takata, M.; Kitamura, H.; Ishikawa, T.; Tada, M.; Yokoyama,T.; Iwasawa, Y. SPring-8 BL36XU: Catalytic Reaction Dynamics for Fuel Cells. *J. Phys.: Conf. Series* **2016**, *712*, 012142-1-4.

(33) Zatoń, M.; Rozière, J.; Jones D. J. Current Understanding of Chemical Degradation Mechanisms of Perfluorosulfonic Acid Membranes and Their Mitigation Strategies: a Review. *Sus. Energy Fuels* **2017**, *1*, 409–438.

(34) Nonnenmann, S. S.; Kungas, R.; Vohs, J.; Bonnell, D. A. Direct In Situ Probe of Electrochemical Processes in Operating Fuel Cells, *ACS Nano* **2013**, *7*, 6330–6336.

(35) Ravel, B.; Newville, M. ATHENA, ARTEMIS, HEPHAESTUS: Data Analysis for X-ray Absorption Spectroscopy using IFEFFIT. *J. Synchrotron Rad*. **2005**, *12*, 537–541.

(36) Ankudinov, A. L.; Ravel, B.; Rehr, J. J.; Conradson, S. D. *Phys. Rev. B* **1998**, *58*, 7565-7576.

Graphical table of contents